Effect of Welding Parameters on the Heat-Affected Zone Hydrogen-Induced Cracking Tendency of a Blast-Resistant Steel

The effect of heat input and preheat on the HAZ hydrogen-induced cracking tendency of BA-160 was evaluated by the implant test

BY X. YUE, X.-L. FENG, AND J. C. LIPPOLD

ABSTRACT

An implant test was used to investigate the effect of welding conditions on the susceptibility of a blast-resistant steel, BlastAlloy-160 (BA-160), to heat-affected zone (HAZ) hydrogen-induced cracking (HIC). The lower critical stress (LCS) was determined using the implant test with different heat input conditions and preheat temperatures. Welding was performed using the gas metal arc process and hydrogen was introduced using an Ar-15%H_2 shielding gas. The microstructure of the coarse-grained heat-affected zone (CGHAZ) of BA-160 was characterized by means of both optical and transmission electron microscopy. The CGHAZ microstructure of the as-welded, low-heat-input welds consisted of untempered martensite with some retained interlath austenite. Increased heat input leads to the formation of lower bainite, decreasing the hardness of the microstructure. Use of preheat for low-heat-input welds also slightly reduced CGHAZ hardness, and the microstructure is predominantly martensite with the possibility of some bainite. It was shown in the implant test results that both increasing heat input and using preheat improved the HIC resistance of the HAZ. The fracture behavior was studied using scanning electron microscopy. It was shown that both welding with high-heat input and applying preheat resulted in an increase in fracture morphology dominated by microvoid coalescence with no intergranular fracture.

Introduction

Steels are currently being used as the principal structural material in naval ship construction, primarily because of their relatively low cost and good combination of mechanical properties. For many years, the U.S. Navy has focused on developing stronger and tougher steels for the hull and deck applications (Refs. 1–3). The projected property requirements for high-strength, blast-resistant naval steels needed for future ship applications is impact fracture toughness above 115 J at –64°C with a yield strength in the range from 1030 to 1240 MPa. These steels should possess good formability and weldability, especially good resistance to heat-affected zone (HAZ) hydrogen-induced cracking (HIC) (Ref. 4).

X. YUE (yuexinosu@gmail.com), *X.-L. FENG, and J. C. LIPPOLD are with the Welding Engineering Program, The Ohio State University, Columbus, Ohio.*

A new steel, BlastAlloy 160 (BA-160), was developed at Northwestern University to meet these rigorous requirements for blast-resistant naval material applications. It was designed based on a theoretical computational materials design concept, using a multiscale materials modeling method and detailed advanced microstructural characterization techniques. It has high yield strength of 1100 MPa (160 ksi) and impact toughness of 176 J at 25°C. The chemical composition of BA-160 is listed in Table 1. The steel heat treatment procedure, as outlined in Table 2, was used to achieve the combination of high strength and toughness. The high strength results from the combined effects of a martensite/bainite matrix, M_2C carbides (where M=Cr, Mo, and V) and copper precipitates, which are in the range of 3–5 nm. High toughness results from the presence of finely dispersed, Ni-stabilized austenite, based on a dispersed phase transformation toughening mechanism. More information on the design and microstructure development of BA-160 can be found in publications by Saha et al. (Refs. 5, 6).

KEYWORDS

High-Strength Steels
Hydrogen-Induced Cracking
Heat Input
Preheat
Implant Test
CGHAZ Microstructure
Fracture Behavior
BA-160

As with most steels developed for shipbuilding applications, one of the primary design objectives for BA-160 is that it should possess good weldability. Among the weldability issues associated with welding high-strength steels, HAZ HIC is one of the biggest concerns, as validated by numerous publications by previous researchers (Refs. 7–15). Heat-affected zone HIC was also referred to as HAZ cold cracking or delayed cracking in the welding literature. Researchers have proposed a number of theories to describe the cracking mechanism. Some of the more popular theories that have evolved over the years include the surface adsorption theory by Petch (Ref. 16), the decohesion theory by Troiano (Ref. 17), and the theory proposed by Beachem stating that fracture behavior is dependent on the combined effect of stress intensity at crack tip and hydrogen concentration (Ref. 18). Even though a unified mechanism for HIC still does not exist, it is generally agreed that the occurrence of HIC in the HAZ of welds in high-strength steels requires the simultaneous presence of a threshold level of hydrogen, a susceptible microstructure, and tensile residual stress (Ref. 19).

In order for the new steel to be welded with good resistance to HAZ HIC, an understanding of the influence of welding

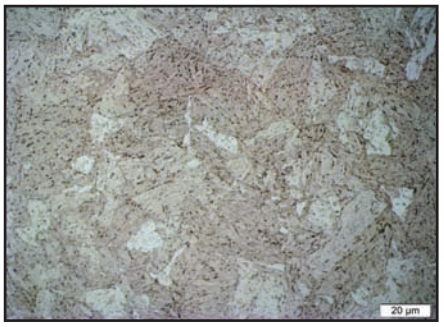

Fig. 1 — Microstructure of the BA-160 base metal, which shows a tempered martensite/bainite matrix with various precipitates dispersed on the matrix.

parameters on the cracking tendency using lab test is needed. In the present study, the implant test was used to evaluate the HAZ HIC tendency of BA-160 under different welding conditions. The influence of heat input and effectiveness of preheat on reducing cracking susceptibility have been investigated using the implant test. The CGHAZ microstructure was characterized using optical and transmission electron microscopy, and the fracture behavior was studied with scanning electron microscopy.

Material and Experimental Procedures

BA-160 was provided in the form of 35-mm- (1.375-in.-) diameter bar stock by QuesTek Innovations LLC, Evanston, Ill. The composition of the material used in this study is listed in Table 1. It was heat-treated following the procedure in Table 2, and the base metal microstructure is shown in Fig 1.

The implant test, which was originally developed by Henri Granjon (Ref. 20), was used in the present investigation to evaluate the HAZ HIC susceptibility. It has been shown to be an effective HAZ HIC test method, which provides a quantitative measure of HIC susceptibility (Refs. 21, 22). The schematic of the implant test, testing system, and implant specimen are shown in Fig. 2A–D. The implant specimens, as shown in Fig. 2D, were machined from the BA-160 steel along the rolling direction of the bar stock, with dimensions shown in Table 3. One end of the implant specimen was 0.5 in. (12.7 mm) long with a 10-32 UNF thread and was inserted into a clearance hole in the center of the specimen plate, with the top of the 10-32 UNF thread section flush with the specimen plate top surface. The other end of the implant specimen was 0.5 in. (12.7 mm) long with a 1/4-20 UNC thread and was threaded into a connection rod of The Ohio State University Modified Implant Testing System (OSU-MITS) so that a constant tensile load could be applied after welding is completed.

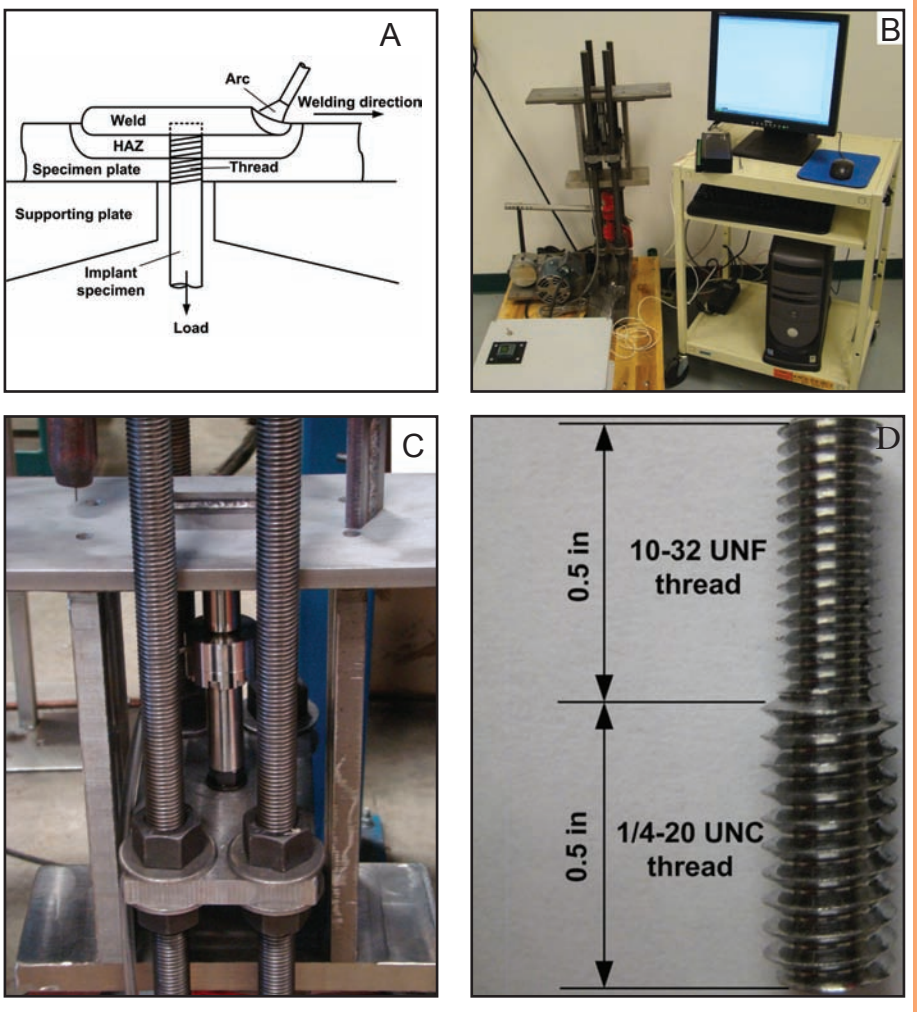

Fig. 2 — The implant test system (OSU-MITS) and specimen. A — Schematic drawing of the implant test; B — full view of the OSU-MITS; C — close-up view showing an implant specimen under loading and an unloaded one on the top right corner ; D — the implant specimen.

A weld bead was deposited using the gas metal arc welding (GMAW) process with 0.047-in.- (1.2-mm-) diameter SuperArc® LA-100 wire (composition shown in Table 1) on the surface of the specimen plate directly over the 10-32 UNF thread and the hole. A low and a high heat input, which were 33 kJ/in. (1.3 kJ/mm) (voltage, 30 V; current, 220 A; travel speed, 12 in./min); and 66 kJ/in(2.6 kJ/mm) (voltage, 30 V; current, 220 A; travel speed: 6 in./min), respectively, were used to evaluate the effect of heat input on the HAZ cracking tendency. In addition, for the low heat input, preheat of 60°, 100°, and 150°C were applied before welding to evaluate the preheat effect on reducing the HIC tendency. Before welding, the specimen plate and implant specimen were heated to 300°C in a heating furnace, then were quickly moved to the OSU-MITS and fixed on the testing system. A Type K thermocou-

Table 1 — Chemical Composition of BA-160 Steel and SuperArc LA-100 (wt-%)

	C	Mn	Si	P	S	Cu	Ni	Cr	Mo	V	Nb	Ti	Al	Zr
BA-160	0.059	0.001	0.015	<0.005	<0.001	3.39	6.8	1.9	0.61	<0.001	<0.001	0.016	0	0
SuperArc LA-100	0.05–0.06	1.63–1.69	0.46–0.50	0.005–0.009	0.002–0.005	0.11–0.14	1.88–1.96	0.04–0.06	0.43–0.45	≤0.01	0	0.03–0.04	≤0.01	≤0.01

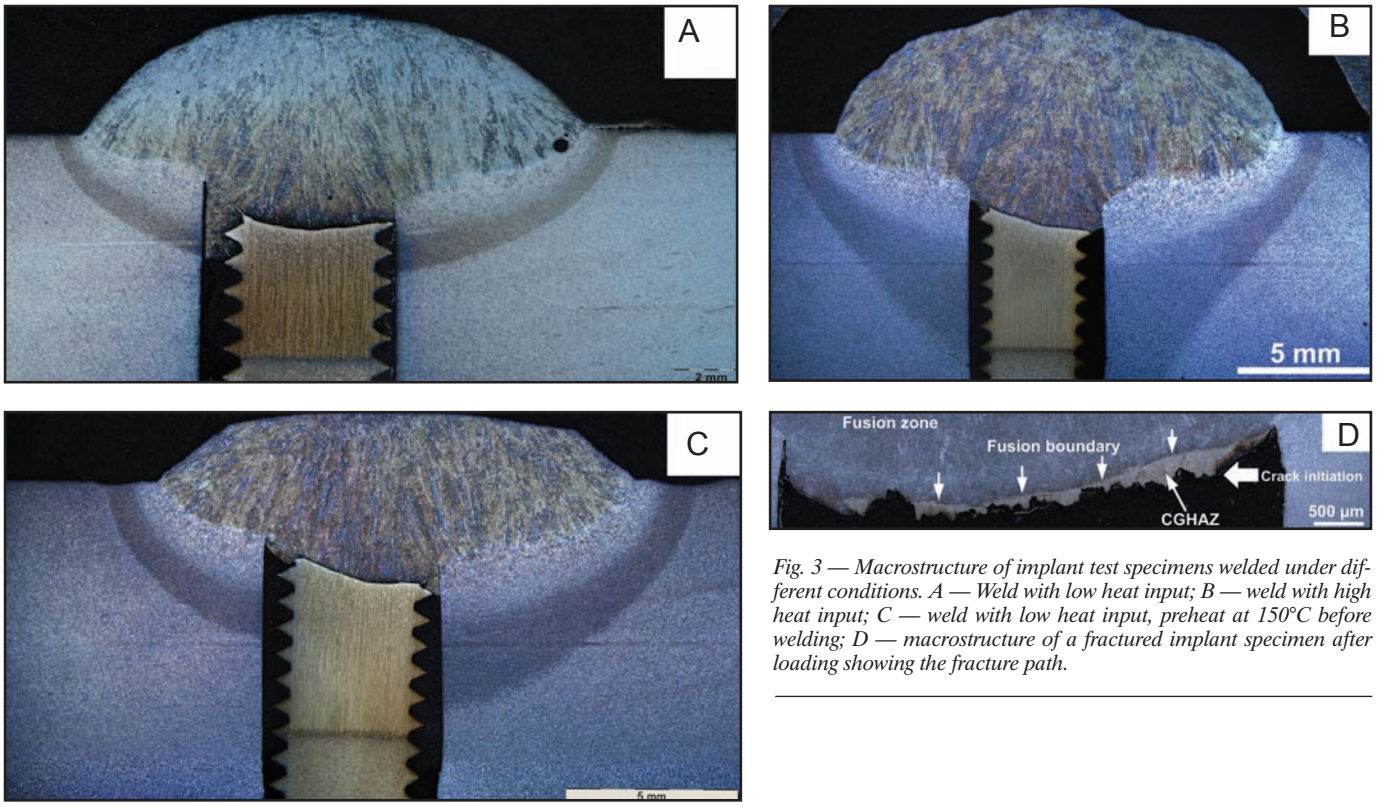

Fig. 3 — Macrostructure of implant test specimens welded under different conditions. A — Weld with low heat input; B — weld with high heat input; C — weld with low heat input, preheat at 150°C before welding; D — macrostructure of a fractured implant specimen after loading showing the fracture path.

Table 2 — Heat Treatment Procedure for BA-160

Step	Temperature,°C	Duration	Post step procedure
1. Austenitization	900	1 h	Water quench
2. Liquid nitrogen hold	–196	30 min	Air warm to room temp
3. Tempering	550	30 min	Water quench
4. Tempering	450	5 h	Air cool to room temp

ple was connected to the data-acquisition system of OSU-MITS and used to measure the temperature of the specimen plate. Welding was started on the preheated specimens once the temperature of the specimen plate dropped to the predetermined preheat temperature. Argon + 15% H_2 shielding gas at a flow rate of 45 ft^3/h (21.2 L/min) was used to introduce sufficient diffusible hydrogen into the weld joint to promote HIC in the HAZ.

A HAZ was created in the 10-32 UNF thread region of the implant specimen after welding. Two minutes after completion of welding, the implant sample was subjected to a static tensile load. The tensile stress was determined by the load divided by the cross-sectional area of the root diameter of the 10-32 thread. The implant sample was free of bending, torsion, or shock loading as a result of the specific design of OSU-MITS. The stress concentration caused by the 10-32 UNF thread forced cracking to occur in the susceptible HAZ region rather than the fusion zone. The data-acquisition system was used to monitor the load and measure the time to failure. To generate the implant test curve, multiple samples were welded with the same welding parameters and subjected to different loads in order to generate a tensile stress vs. time to failure relationship. The highest stress at which no failure occurs after 24-h loading was defined as the lower critical stress (LCS) (Ref. 23), which was taken as an index to determine susceptibility to HIC in the HAZ.

Metallographic samples were sectioned perpendicular to the welding direction along the axis of the implant specimens. Following mounting and polishing, they were etched with 5% nital and examined using optical microscopy. Transmission electron microscope (TEM) samples were evaluated in a Philips CM200 TEM operated at 200 kV. The fracture surface of the implant samples was examined under a Philips XL30F ESEM. Vickers hardness measurements were conducted along the axis of the implant samples using a 1-kg load, in accordance with ASTM E 384-10.

Results and Discussion

Weld Macrostructure

The weld macrostructures under different welding conditions are shown in Fig. 3A–C. It can be seen that a distinct HAZ was created on the 10-32 UNF thread region for all three weld conditions. When increasing heat input (Fig. 3B) and using preheat (Fig. 3C), the area of the fusion zone is larger as compared to that welded with low heat input (Fig. 3A), and the width of the HAZ becomes larger when high heat input or preheat was used. Figure 3D shows a fractured implant specimen sectioned to reveal the HIC fracture path. The fusion boundary separating the fusion zone and HAZ can be clearly seen. The crack initiates from the root of the unfused thread and propagates through the CGHAZ approximately 100–300 microns away from the fusion boundary. In most steels, the CGHAZ is the most susceptible to HAZ HIC since it has the largest prior austenite grain size and high hardness (Refs. 24–26).

Vickers Hardness Test Results

Hardness is a direct indication of a different microstructure formed, and is an important factor that influences the HAZ HIC tendency. Therefore, Vickers hardness measurements were taken along the axis of the implant specimens welded under different conditions, starting in the fusion zone and running through the HAZ

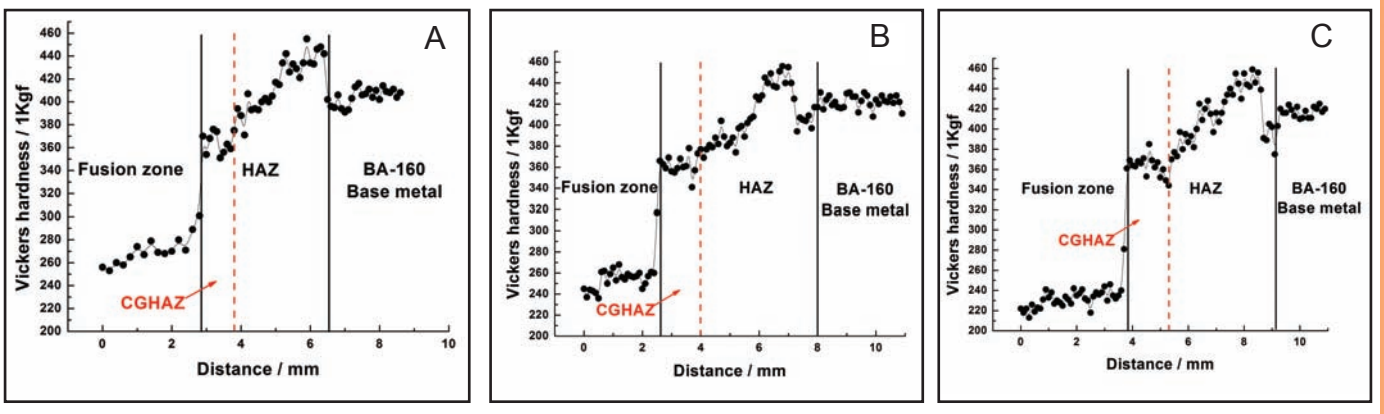

Fig. 4 — Vickers hardness measurements taken along the axis of the implant specimen. A — Weld with low heat input; B — weld with high heat input; C — weld with low heat input, preheat at 150°C before welding.

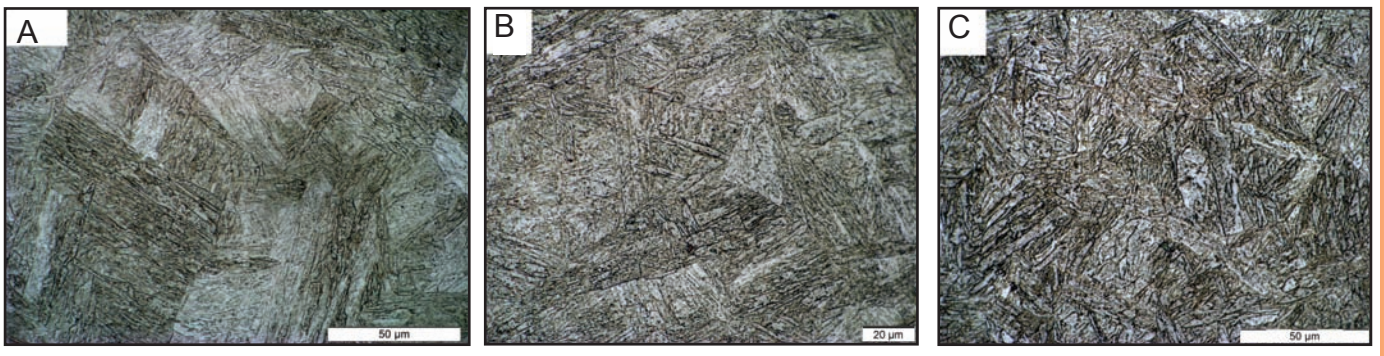

Fig. 5 — Optical micrographs for the CGHAZ of BA-160. A — Weld with low heat input; B — weld with high heat input; C — weld with low heat input, preheat at 150°C before welding.

to the unaffected base metal, as shown in Fig. 4A–C. The HAZ is indicated in the three hardness plots as the region between the two black solid lines. The red dotted line is the approximate boundary between the CGHAZ and its adjacent fine-grained HAZ (FGHAZ).

It can be seen in all three hardness traverses that the hardness of the fusion zone is lower compared to HAZ and base metal. And when welded with high heat input or using preheat, the fusion zone hardness decreases as compared to using low heat input without preheat, indicating different cooling rates under different welding conditions lead to the formation of different microstructures in the fusion zone.

For all three conditions, the hardness of the CGHAZ is actually the lowest across the HAZ. This is attributed to the difference in lath martensite morphology and Cu precipitation behavior in different HAZ regions as a result of different thermal cycles experienced (Ref. 4). Even though the CGHAZ has the lowest HAZ hardness, it is the most HIC-susceptible region, as shown in Fig. 3D. When using low heat input as shown in Fig. 4A, the average CGHAZ hardness is 370 $HV_{1.0}$, and it slightly decreases to an average of 358 $HV_{1.0}$ when welded with high heat input, and to an average of 363 $HV_{1.0}$ when using preheat at 150°C. The hardness results are summarized in Table 4.

Table 3 — Specimen Plate/Implant Specimen Dimensions

Specimen plate	
Material	A36 steel
Plate thickness in. (mm)	0.5 (12.7)
Plate width in. (mm)	2 (50.8)
Plate length in. (mm)	4 (101.6)
Length of test bead in. (mm)	3.5 (88.9)
Hole diameter in. (mm)	0.201 (5.1)
Implant specimen	
Material	BA-160
Total length of implant specimen in. (mm)	1 (25.4)
Type of thread	10-32 UNF
Pitch in. (mm)	1/32 (0.79)
Major diameter in. (mm)	0.1900 (4.83)
Minor diameter in. (mm)	0.1517 (3.85)
Thread length in. (mm)	0.5 (12.7)
Thread angle	60 deg
Thread root radius in. (mm)	0.004 (0.1)

Weld CGHAZ Microstructure

Since cracking occurs in the CGHAZ region adjacent to the fusion boundary, the CGHAZ microstructure will influence the cracking tendency. Therefore, in this study, the CGHAZ microstructure of BA-160 under different welding conditions was characterized.

It is known that cooling rate influences the phase transformation behavior. Using an online weld modeling tool, EWI E-Weld Predictor™ (Ref. 27), the $t_{8/5}$, which represents the cooling time from 800° to 500°C, is estimated to be 3.5, 7.3, and 4.8 s

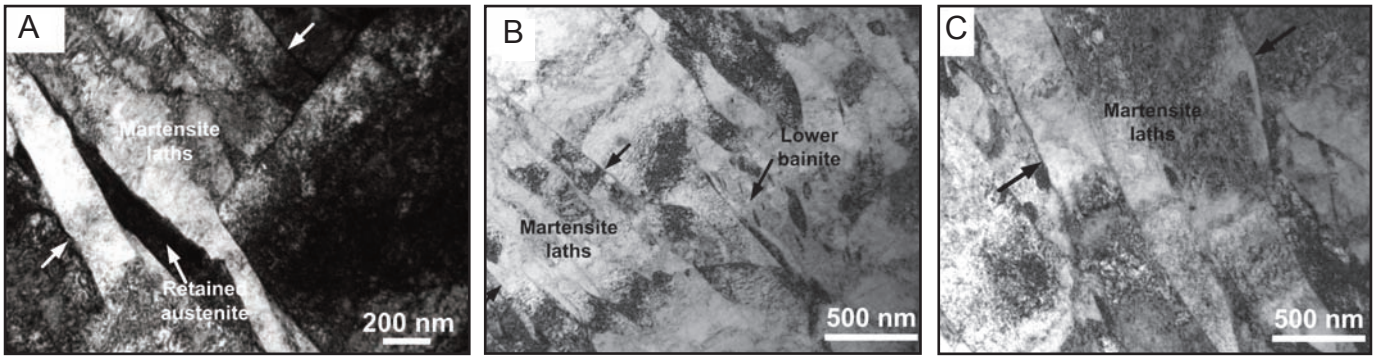

Fig 6 — Bright-field TEM micrographs for the CGHAZ of BA-160. A — Weld with low heat input; B — weld with high heat input; C — weld with low heat input, preheat at 150°C before welding.

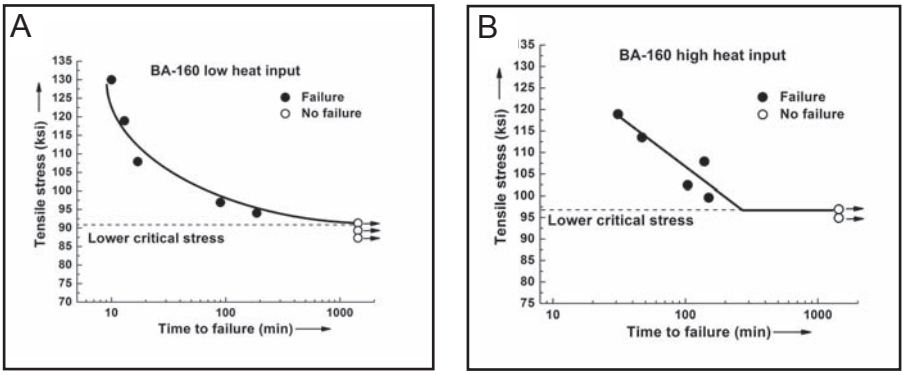

Fig. 7 — Implant test results for BA-160. A — Weld with low heat input; B — weld with high heat input.

for low heat input, high heat input, and using preheat of 150°C, respectively. Note that the calculated $t_{8/5}$ is only an approximate value; however, it can be clearly seen that both welding with high heat input and applying preheat decrease cooling rate as compared to welding with low heat input.

It is shown in the optical micrographs in Fig. 5A–C that no diffusion-controlled transformation products such as ferrite or pearlite can be observed, and martensite is the predominant feature. The predominant formation of martensite in the CGHAZ is primarily due to the high alloy addition in BA-160, which results in high hardenability as indicated by the high carbon equivalent (CE_{AWS} = 1.24) (Ref. 28). The CGHAZ microstructure forming at different welding conditions was further investigated under higher magnification TEM, as shown in Fig. 6A–C. A packet of martensite laths can be observed in Fig. 6A. Because of the low carbon content in BA-160 (0.059 wt-%), the martensite formed in the CGHAZ is lath martensite, which can also be confirmed by the existence of a dislocation network within the martensite laths. The dark region between martensite laths is retained austenite.

The existence of retained austenite results from the high-nickel addition (6.8 wt-%) in BA-160, which is an effective austenite stabilizer depressing the M_s and M_f temperatures. It was determined that for BA-160 CGHAZ, M_s is 355°C and M_f is 178°C (Ref. 29). During the welding cooling process, austenite rich in Ni did not transform to martensite. It was stabilized to the ambient temperature and therefore results in incomplete austenite transformation to martensite, even under fast cooling rates. At higher heat input, lower bainite is formed in the CGHAZ under slower cooling rates, which can be confirmed by the formation of intralath plate-like cementite precipitates within the bainite laths, as shown in Fig. 6B. The cementite precipitates are oriented at a preferential angle with the primary bainite lath growth direction, and this is the characteristic feature distinguishing lower bainite from upper bainite or lath martensite (Ref. 30). Note that lower bainite represents only a small fraction of the CGHAZ microstructure, and because of the thin laths and limited amount, it cannot be resolved in the optical microscope. Martensite laths free of intralath cementite can also be seen in Fig. 6B and C, and it was found that less retained austenite was present with increasing heat input or applying preheat. The average Vickers hardness of the CGHAZ with low heat input is 370 $HV_{1.0}$ and decreases to 358 $HV_{1.0}$ with the increase in heat input and to 363 $HV_{1.0}$ with applying preheat of 150°C. Due to the hardness decrease when using preheat, it is postulated that a small quantity of lower-hardness bainite may form in the CGHAZ when welding with preheat of 150°C because of the lower cooling rate as compared to welding with low heat input.

Table 4 — Summary of Microstructure, Hardness, and Implant Test Results for Different Welding Conditions for BA-160

Welding Conditions	Low HI (33 kJ/in.)	High HI (66 kJ/in.)	Low HI (33 kJ/in.), preheat at 60°C	Low HI (33 kJ/in.), preheat at 100°C	Low HI (33 kJ/in.), preheat at 150°C
CGHAZ microstructure	M	M+B	M	M	M+(B)[a]
CGHAZ Hardness (Avg)[b]	370	358	368	366	363
Implant test LCS	91 ksi (627 MPa)	96 ksi (661 MPa)	94 ksi (648 MPa)	103 ksi (710 MPa)	107 ksi (737 MPa)

(a) M represents martensite; B represents bainite; (B) represents possible formation of bainite in the microstructure.
(b) Avg means the average hardness of the CGHAZ, which is determined by taking the average of hardness data points in the CGHAZ region together. The approximate boundary of CGHAZ is determined by metallographic observation.

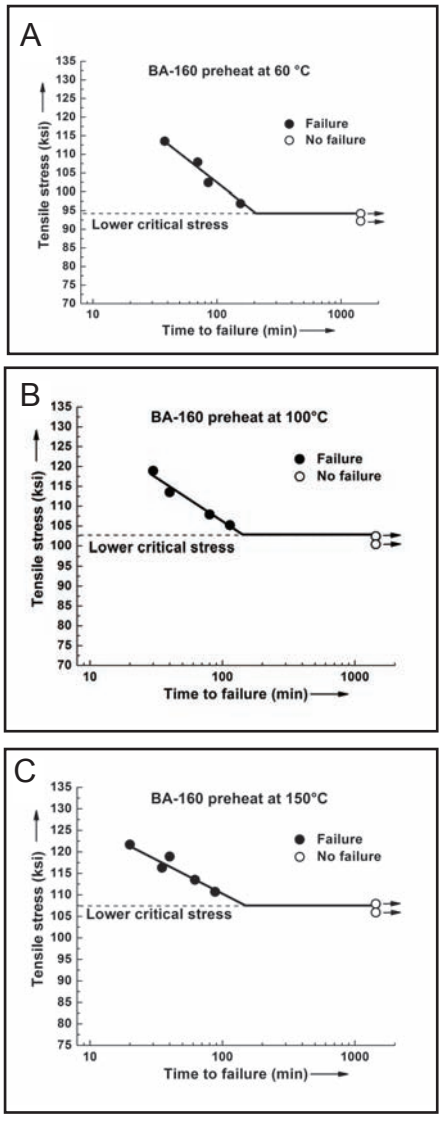

Fig. 8 — Implant test results for BA-160, weld with low heat input. A — Preheat at 60°C; B — preheat at 100°C; C — preheat at 150°C.

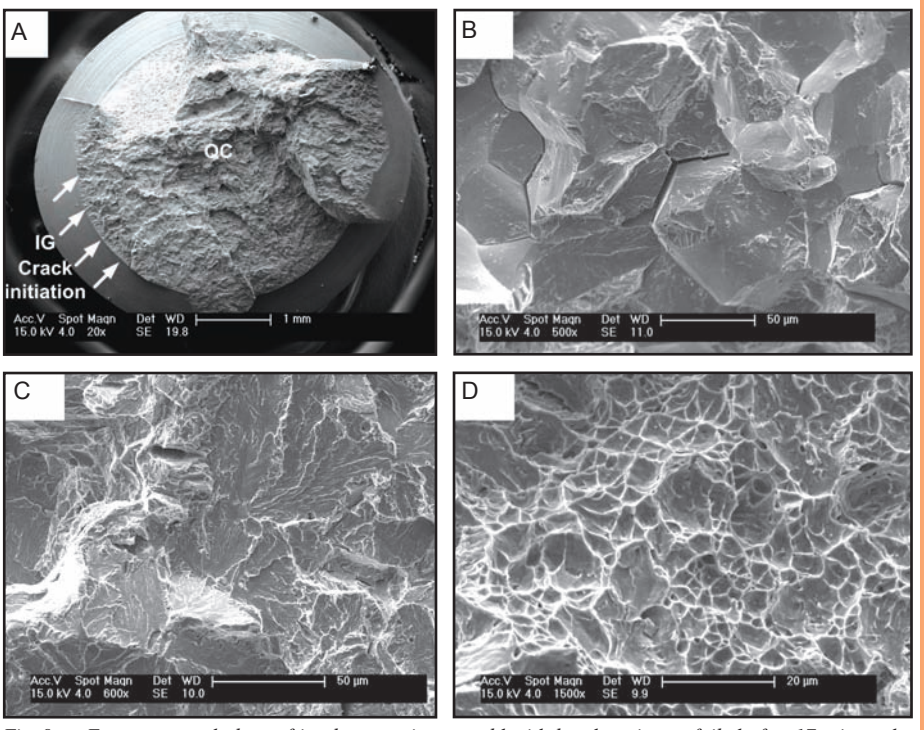

Fig. 9 — Fracture morphology of implant specimen, weld with low heat input, failed after 17 min under tensile stress of 107.9 ksi. A — General fracture appearance; B — intergranular; C — quasi-cleavage; D — microvoid coalescence.

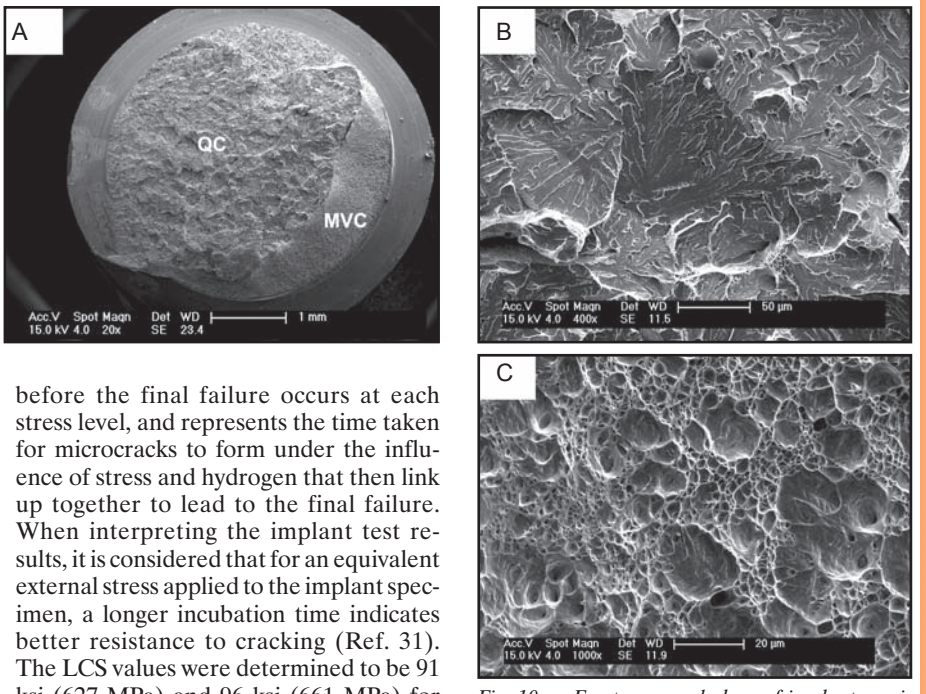

Fig. 10 — Fracture morphology of implant specimen, weld with high heat input, failed after 139 min under tensile stress of 107.9 ksi. A — General fracture appearance; B — quasi-cleavage; C — microvoid coalescence.

Effect of Heat Input on BA-160 HAZ Hydrogen-Induced Cracking Tendency

Heat input is a factor that influences the HIC tendency. Different heat inputs will result in different cooling rates and, as shown in Figs. 5 and 6, lead to the formation of different microstructures in the HAZ during cooling after welding. As discussed in the previous section, the low heat input resulted in a harder microstructure as compared to the high heat input.

The implant test results for the two heat inputs are shown in Fig. 7A and B. The lower critical stress (LCS) for each welding condition was determined. Lower critical stress is defined as the maximum stress at which cracking does not occur after 24-h loading under the influence of diffusible hydrogen. Therefore, the higher the LCS, the better is the resistance to HIC. It can be seen in the implant test results that an incubation time is observed before the final failure occurs at each stress level, and represents the time taken for microcracks to form under the influence of stress and hydrogen that then link up together to lead to the final failure. When interpreting the implant test results, it is considered that for an equivalent external stress applied to the implant specimen, a longer incubation time indicates better resistance to cracking (Ref. 31). The LCS values were determined to be 91 ksi (627 MPa) and 96 ksi (661 MPa) for low and high heat input, respectively, as listed in Table 4. The increase in LCS when using high heat input indicates that increasing heat input when welding BA-160 steel reduces the tendency for HIC in the CGHAZ. The reduction in cracking susceptibility when using high heat input can also be seen by the comparison of the incubation time before failure. When the applied stress is 107 ksi (737 MPa), the incubation time for the low heat input is 17 min, while it increases to 139 min for the high heat input.

Clearly, the reduced HIC susceptibility for the CGHAZ of BA-160 when increasing heat input is the difference in microstructure as a result of slower cooling rates. The lower hardness microstructure of the mixed martensite and lower bainite formed at slow cooling rates has a better resistance to cracking as compared to the

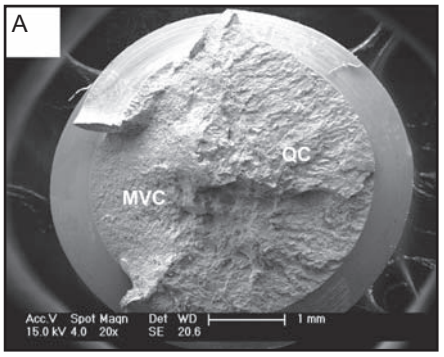

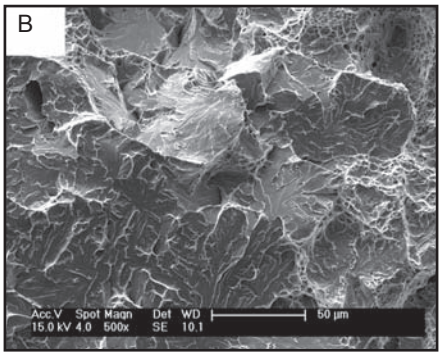

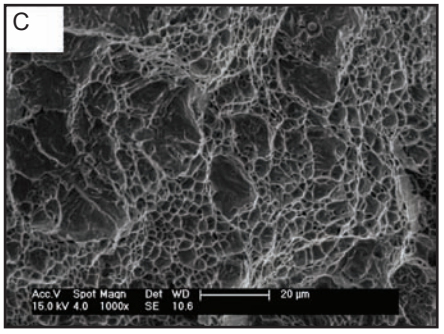

Fig. 11 — Fracture morphology of implant specimen weld with low heat input and preheat of 100°C, failed after 80 min under tensile stress of 107.9 ksi. A — General fracture appearance; B — quasi-cleavage; C — microvoid coalescence.

higher hardness martensitic microstructure formed at low heat input.

However, it should be noted that in real welding practice, reducing HAZ HIC tendency by using a very high heat input may either not be practical or lead to severe grain coarsening, which may either reduce toughness or cause softening. As a result, the determination of heat input should also consider other factors.

Effect of Preheat on Reducing BA-160 HAZ Hydrogen-Induced Cracking Tendency

Preheat and/or interpass temperature control are used as effective means in actual welding practice to alleviate HAZ HIC in steels. First, preheating the steel before welding will lead to a slower cooling rate, which generally results in the formation of lower hardness microstructures such as ferrite, pearlite, and/or bainite in the HAZ. These transformation products are less susceptible to HIC as compared to hard and brittle martensite. Second, preheat can drive off any preexisting moisture and promote longer weld cooling times both of which reduce the diffusible hydrogen content in the HAZ. The reduction of diffusible hydrogen will thereby reduce the cracking tendency. Since BA-160 is designed as a structural steel for naval ship applications, it is likely that high-restraint, high-hydrogen conditions will be encountered during fabrication. Therefore, it is necessary to investigate using the lab test if preheat is effective to alleviate HAZ HIC when welding BA-160.

In the present study, implant testing was conducted with preheat temperatures of 60°, 100°, and 150°C to evaluate the preheat effect on reducing the cracking tendency. The implant test results are shown in Fig. 8A–C. It can be seen that with preheat before welding, all three curves show that the incubation time prior to failure is longer than that without preheat at equivalent tensile stress levels, as compared to Fig. 7A, indicating applying preheat reduces HAZ cracking tendency. This is because applying preheat can reduce the diffusible hydrogen content, and thereby a longer incubation time is required to reach the critical hydrogen level to cause cracking to occur. This is one evidence indicating that preheat is effective to alleviate the HAZ HIC cracking tendency for BA-160.

The LCS with preheating at 60°C was determined to be 94 ksi (648 MPa), which is slightly higher as compared to 91 ksi (627 MPa) without preheat. Increasing the preheat temperature to 100°C, the LCS was increased to 103 ksi (710 MPa), and this was also with a concomitant increase in incubation time. By further increasing the preheat temperature to 150°C, the LCS was increased to 107 ksi (737 MPa). This clearly indicates that increasing preheat temperature is beneficial to reduce HAZ cracking tendency for BA-160. However, increasing preheat temperature to 150°C to reduce cracking was not so effective compared with the 9-ksi LCS increase from preheat at 60° to 100°C. Based on the implant test results, it is shown that applying preheat and increasing preheat temperature are beneficial to reduce the cracking tendency for BA-160. One reason is that applying preheat results in a lower cooling rate, which leads to the formation of a lower hardness microstructure in the CGHAZ as found in the Vickers hardness test results. The other reason is that preheat is effective to reduce the diffusible hydrogen level in the HAZ as discussed previously.

Effect of Welding Parameters on Fracture Behavior

The fracture surfaces of the implant specimens welded under different conditions were studied using SEM to analyze the effect of welding parameters on fracture behavior. The SEM fractographs of the BA-160 implant specimens are presented in Figs. 9–11. For the three welding conditions, the fracture surface studied was from the implant specimens failed at the same tensile stress (107.9 ksi) for the purpose of comparison.

Figure 9A shows the general fracture appearance of a BA-160 implant specimen with low heat input, and regions with different fracture modes are shown in Fig. 9B–D at higher magnification. Coarse intergranular (IG) failure, as shown in Fig. 9B, is only observed in the region close to the root of the thread where the crack initiates. A quasi-cleavage (QC) mode, as shown in Fig. 9C, constitutes the majority of the fracture surface. Microvoid coalescence (MVC) is observed in only a small area close to the final failure region, as shown in Fig. 9D.

The fracture morphology of a specimen from a high-heat-input weld is shown in Fig. 10A–C. There is no faceted, coarse IG fracture observed on the fracture surface, in contrast to the fracture surface with low-heat input. Quasi-cleavage is also the predominant feature, as shown in Fig. 10A and B. However, the region of MVC becomes larger as compared to that of low heat input.

Figure 11A–C shows the fracture morphology with low heat input and a preheat level of 100°C. Similar to Fig. 10A, no obvious IG failure can be observed at the crack initiation site. The crack initiates and propagates with QC mode for a long distance, and then the fracture mode changes to MVC.

It is found that using both high heat input and preheat eliminate the IG fracture mode, and increase the MVC area on the fracture surface as compared to the low-heat-input condition. This is an indication that increasing heat input and using preheat improve HIC resistance. And this is the result of formation of lower hardness microstructure in the CGHAZ with decreasing cooling rate, and also because of the preheating effect to drive off hydrogen from the weld pool.

Conclusions

1. Using low-heat-input welding conditions (33 kJ/in.), the CGHAZ microstructure of BA-160 is lath martensite with retained austenite. With high heat input (66 kJ/in.), lower bainite forms in the CGHAZ. The mixture of martensite and lower bainite has a lower hardness as com-

pared to the martensitic microstructure formed with low heat input.

2. When preheat of 150°C is applied in conjunction with the low-heat-input welding conditions, the hardness is decreased and the microstructure is a mixture of martensite and a possibly small fraction of bainite.

3. Implant test results show that at equivalent stress levels, the incubation time prior to failure is longer when high heat input is used as compared to low heat input. The lower critical stress (LCS) was found to increase from 91 ksi (627 MPa) with low heat input to 96 ksi (661 MPa) with high heat input. Both the longer incubation time present and increase in the LCS indicate that using higher heat input reduces the HAZ cracking tendency for BA-160.

4. The LCS was determined to be 94, 103, and 107 ksi (648, 710, and 737 MPa) with preheat levels of 60°, 100°, and 150°C, respectively. The LCS with preheat is higher than that without preheat. And the incubation time at equivalent tensile stress is also longer than that without preheat. Both indicate preheating can effectively reduce the tendency for HIC in BA-160.

5. Intergranular, quasi-cleavage, and microvoid coalescence fracture modes were observed on the fracture surface of implant samples from low-heat-input welds. Only quasi-cleavage and microvoid coalescence were observed on the fracture surface when using high heat input and applying preheat. The elimination of IG and increase in MVC area on the fracture surface correlated well with LCS values and indicated better resistance to cracking.

Acknowledgments

The authors gratefully acknowledge the financial support of the Office of Naval Research, Award No. N000140811000. Grant Officers: Dr. Julie Christodoulou and Dr. William Mullins. The authors would like to thank Johnnie DeLoach, Matthew Sinfield, and Jeffrey Farren with the Naval Surface Warfare Center Carderock Division, West Bethesda, Md., for valuable discussions regarding the weldability of naval steels. Thanks are extended to Prof. Gregory Olson's research group at Northwestern University for collaboration on this research project and QuesTek Innovations LLC for providing the BA-160 steel. Dr. Yuping Yang with EWI is acknowledged for providing access to the E-Weld Predictor™. Dejian Liu and Geoffrey Taber are thanked for their constructive ideas and assistance with building the implant testing system.

References

1. Czyryca, E. J. 1993. Advances in high strength steel technology for naval hull construction. *Key Engineering Materials* 84-85: 491–520.

2. Czyryca, E. J., Link, R. E., Wong, R. J., Aylor, D. A., Montemarano, T. W., and Gudas, J. P. 1990. Development and certification of HSLA-100 steel for naval ship construction. *Naval Engineers Journal* 102(3): 63–82.

3. Montemarano, T. W., Sack, B. P., Gudas, J. P., Vassilaros, M. G., and Vanderveldt, H. H. 1986. High strength low alloy steels in naval construction. *Journal of Ship Production* 2(3): 145–162.

4. Yu, X., Caron, J. L., Babu, S. S., Lippold, J. C., Isheim, D., and Seidman, D. N. 2010. Characterization of microstructural strengthening in the heat-affected zone of a blast-resistant naval steel. *Acta Materialia* 58: 5596–5609.

5. Saha, A., and Olson, G. B. 2007. Computer-aided design of transformation toughened blast resistant naval hull steels: Part I. *Journal of Computer-Aided Materials Design* 14: 177–200.

6. Saha, A., Jung, J., and Olson, G. B. 2007. Prototype evaluation of transformation toughened blast resistant naval hull steels: Part II. *Journal of Computer-Aided Materials Design* 14: 201–233.

7. Gedeon, S. A., and Eagar, T. W. 1990. Thermochemical analysis of hydrogen absorption in welding. *Welding Journal* 69(7): 264-s to 271-s.

8. Devletian, J. H., and Fichtelberg, N. D. 2001. Controlling hydrogen cracking in shipbuilding. *Welding Journal* 80(11): 46– 52.

9. Rowe, M. D., Nelson, T. W., and Lippold, J. C. 1999. Hydrogen-induced cracking along the fusion boundary of dissimilar metal welds. *Welding Journal* 78(2): 31-s to 37-s.

10. Park, Y. D., Maroef, I. S., Landau, A., and Olson, D. L. 2002. Retained austenite as a hydrogen trap in steel welds. *Welding Journal* 81(2): 27-s to 35-s.

11. Brauser, S., and Kannengiesser, Th. 2010. Hydrogen absorption of different welded duplex steels. *International Journal of Hydrogen Energy* 35: 4368–4374.

12. Maroef, I., Olson, D. L., Eberhart, M., and Edwards, G. R. 2002. Hydrogen trapping in ferritic steel weld metal. *International Materials Reviews* 47(4): 191–223.

13. DeLoach, J. J., Null, C., Flore, S., and Konkol, P. 1999. The right welding wire could help the U.S. Navy save millions. *Welding Journal* 78(6): 55–58.

14. Cullison, A. 1994. Two paths, one goal: A consumable to weld HSLA 100. *Welding Journal* 73(1): 51–53.

15. Moon, D. W., Fonda, R. W., and Spanos, G. 2000. Microhardness variations in HSLA-100 welds fabricated with new ultralow-carbon weld consumables. *Welding Journal* 79(10): 278-s to 285-s.

16. Petch, N. J., and Stables, P. 1952. Delayed fracture of metals under static load. *Nature* 169(4307): 842–843.

17. Troiano, A. R. 1960. The role of hydrogen and other interstitials in the mechanical behavior of metals. *Transactions of American Society for Metals* 52: 54–80.

18. Beachem, C. D. 1972. A new model for hydrogen-assisted cracking (Hydrogen embrittlement). *Metallurgical Transactions* 3: 437–451.

19. Kou, S. 2003. *Welding Metallurgy*. pp: 410–417, Hoboken, N.J.: John Wiley & Sons, Inc.

20. Granjon, H. 1969. The implants method for studying the weldability of high strength steels. *Metal Construction* and *British Welding Journal* 1(11): 509–515.

21. Yue, X., and Lippold, J. C. 2013. Evaluation of heat-affected zone hydrogen-induced cracking in Navy steels. *Welding Journal* 92(1): 20-s to 28-s.

22. Gedeon, S. A., and Eagar, T. W. 1990. Assessing hydrogen-assisted cracking fracture modes in high-strength steel weldments. *Welding Journal* 69(6): 213-s to 220-s.

23. AWS B4.0:2007, *Standard Methods for Mechanical Testing of Welds*. pp: 67–71. Miami, Fla.; American Welding Society.

24. Nawrocki, J. G., DuPont, J. N., Robino, C. V., and Marder, A. R. 2001. The postweld heat treatment response of simulated coarse-grained heat-affected zones in a new ferritic steel. *Metallurgical and Materials Transactions A* 32A: 2585–2594.

25. Yue, X., Lippold, J. C., Alexandrov, B. T., and Babu, S. S. 2012. Continuous cooling transformation behavior in the CGHAZ of naval steels. *Welding Journal* 91(3): 67-s to 75-s.

26. Spanos, G., Fonda, R. W., Vandermeer, R. A., and Matuszeski, A. 1995. Microstructural changes in HSLA-100 steel thermally cycled to simulate the heat-affected zone during welding. *Metallurgical and Materials Transactions A* 26A: 3277–3293.

27. Zhang, W., and Yang, Y. P. 2009. Development and application of online weld modeling tool. *Welding in the World* 53(1/2): 1–9.

28. Yue, X., Feng, X. L., and Lippold, J. C. 2013. Quantifying heat-affected zone hydrogen-induced cracking in high-strength naval steels. *Welding Journal* 92(9): 265-s to 273-s.

29. Caron, J. L., Babu, S. S., and Lippold, J. C. 2011. Welding-induced microstructure evolution of a Cu-bearing high-strength blast-resistant steel. *Metallurgical and Materials Transactions A* 42A: 4015–4031.

30. Bhadeshia, H. K. D. H. 2001. Bainite in steels: Transformations, microstructure and properties. pp. 63–75. London, UK: IOM Communications Ltd.

31. Dickinson, D. W., and Ries, G. D. 1979. Implant testing of medium to high strength steel — A model for predicting delayed cracking susceptibility. *Welding Journal* 59(7): 205-s to 211-s.